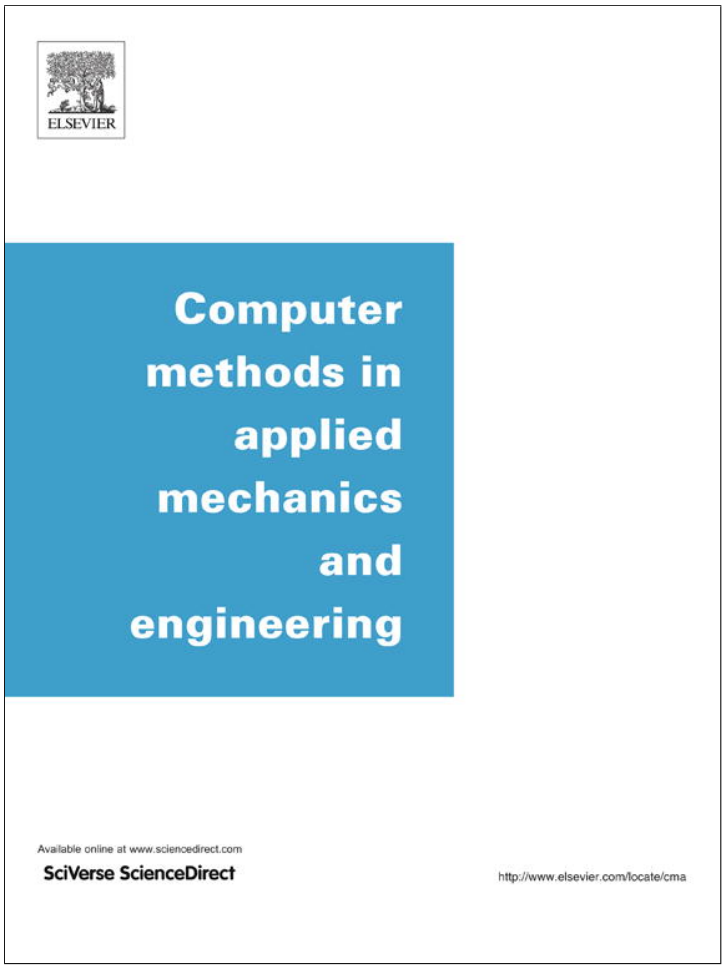

Comput. Methods Appl. Mech. Engrg. 259 (2013) 64–76

Contents lists available at SciVerse ScienceDirect

Comput. Methods Appl. Mech. Engrg.

journal homepage: www.elsevier.com/locate/cma

Generalized formulation for estimating pressure drop in fully-developed laminar flow in singly and doubly connected channels of non-circular cross-sections

Manoj Kumar Moharana [1], Sameer Khandekar *

Department of Mechanical Engineering, Indian Institute of Technology Kanpur, Kanpur, UP 208016, India

ARTICLE INFO

Article history:
Received 23 November 2012
Received in revised form 3 March 2013
Accepted 6 March 2013
Available online 24 March 2013

Keywords:
Fully developed internal laminar flow
Arbitrary cross-sectional ducts
Pressure drop
Poiseuille number
Wall shear stress
Boundary collocation technique

ABSTRACT

Fully developed internal laminar flow through both, singly- and doubly-connected ducts of arbitrary cross-sections, is investigated using a two-dimensional semi-analytical technique in which the condition at the inner/outer arbitrarily defined peripheral boundary of the ducts is matched by a collocation technique. This boundary collocation technique has been applied and validated for (a) singly-connected ducts of standard cross-sectional shapes such as square, circular, etc., (b) a variety of complicated singly-connected duct cross-sectional geometries and, (c) two principal variations of the doubly-connected ducts (i) annular duct having an arbitrary outside perimeter while the internal core perimeter is circular, and (ii) annular duct having a circular outside perimeter while the internal core perimeter is arbitrarily shaped. The proposed model is only a function of geometrical parameters of the duct cross-section. Fluid velocity contours, shear stress distribution along the duct walls and the friction factor (Poiseuille number) has been estimated with this technique and validated against existing solutions for several standard cross-sections and found to be in excellent agreement. Several arbitrary shapes have been considered for analysis. As most micro-fabrication techniques normally do not produce mathematically well-defined or ideal geometries, an experimental test case is also presented wherein, the application of the present methodology in accurately predicting the fully-developed velocity profile, and therefore the net pressure drop, in a microchannel etched on a silicon substrate, is discussed. This simple and universally applicable semi-analytical technique substantially improves the overall predictions for real-time geometries. The critical nuances of successful application of this technique are outlined.

1. Introduction

Conventionally, a circular duct is preferred for internal transport of fluids due to its various advantages including, ease of availability, high pressure sustaining capability and least perimeter for a given cross-section area, amongst others. In recent years though, there is a rapid growth of micro-fluidic systems wherein, due to the variety of manufacturing routes employed for their fabrication, non-circular channels have come into vogue. At these small length scales, quite frequently, due to the inherent limitations of the manufacturing techniques, the cross-sectional shape may also be somewhat irregular than standard geometries such as rectangular, square, circular, ellipsoidal, etc. For example, wet chemical etching of metals is often anisotropic and leads to corner geometries of channels and ducts which do not conform to strict orthogonality or well defined point vertex [1]. Similarly, profiles of materials cut by laser ablation tend to have an inverted bell shape due to the Gaussian distribution of the beam, rather than unique radii of curvature [2]. The small dimensions of microfluidic devices also limit most flows to the laminar fully-developed domain. Occasionally, specific transport goals also necessitate irregular channel geometries, which, depending on wall shapes can provide enhanced transverse mixing features, extended surface conjugate heat transfer, control on transition to turbulence, specific reactivity and cell immobilization features [3]. Benchmarking of pressure drop due to laminar fully developed flow taking place in such 'arbitrary-shaped', non-circular cross section channels is a challenge. Most correlations and semi-analytical or analytical solutions of velocity profiles are confined to regular shape(s) only.

Classical literature is abundant with several analytical and semi-analytical solutions for laminar flow through non-circular channels, as has been critically reviewed in [4–6]. While circular channels have complete symmetry in the angular direction, many other complex cross-sectional shapes are possible and are indeed

* Corresponding author. Tel.: +91 512 2597038; fax: +91 512 2597408.
E-mail addresses: mkmoharana@gmail.com (M.K. Moharana), samkhan@iitk.ac.in, samkhan.iitk@gmail.com (S. Khandekar).
[1] Present address: National Institute of Technology Rourkela, Rourkela 769008, Odisha, India. Tel.: +91 8895593400.

0045-7825/$ - see front matter © 2013 Elsevier B.V. All rights reserved.
http://dx.doi.org/10.1016/j.cma.2013.03.005

Nomenclature

a	semi major axis of an ellipse
A	area of cross-section
$\overline{A}$	dimensionless area of cross-section
$A', B', C', D', A_k, B_k, C_k, D_k, \lambda_k$	integral constants in general solution Eq. (9)
b	semi minor axis of an ellipse
D	diameter
f	friction factor
F_j	right-hand vector in a system of linear equations resulting from simple collocation
G_{jk}	matrix in a system of linear equation resulting from simple collocation
h	height of trapezoidal channel
I	integration as defined in the Appendix A
I_p	polar moment of inertia
I_p^*	specific polar moment of inertia
ℓ	characteristic length scale
L	length scale used for defining Re
$\overline{L}$	ratio of L and ℓ
M	number of collocation points, number of terms considered in the series expansion in Eq. (22)
N	number of symmetric segments in π
p	pressure
P	perimeter
Po	Poiseuille number
r	radius, radial coordinate
r_s	distance of the duct periphery from the origin of the $r-\theta$ coordinate system
R	dimensionless radius variable
$\overline{R}$	dimensionless form of r_s
Re	Reynolds Number
u	velocity of fluid
U	dimensionless velocity as defined in Eq. (7)
$\bar{u}$	average velocity of fluid
$\overline{U}$	dimensionless average velocity as defined in Eq. (7)
Y_k	unknown coefficients
z	transverse coordinate

Greek symbols

θ	angle, angular coordinate
ϕ	side angle of a trapezoidal duct
μ	dynamic viscosity
ε	aspect ratio
ρ	density of fluid
τ	shear stress
$\overline{\tau}$	dimensionless shear stress

Subscripts

h	hydraulic
i	inner
o	outer
p	polar
r	radial component
sym	symmetry
z	transverse component
θ	angular component

being considered for various technological applications, which do not confirm to such universal forms of symmetry. Generalized analytical solutions for hydrodynamics of the flow in ducts having such complicated cross-sectional shapes are limited. With the advent of microfluidics and more frequent occurrence of ensuing intricate cross-sectional geometries in internal convective flow situations, there is a renewed interest to address this issue.

Shah [7] used a least-square matching technique to analyze fully developed laminar fluid flow in singly-connected ducts and predicted Poiseuille number in rectangular, rhombic, trapezoidal, isosceles triangular, rounded corner equilateral triangular and sine ducts. Each particular case was separately handled through tabulated coefficients. Later, Yilmaz [8] generalized the methodology, as given by Shah [7], by developing a correlation scheme for fully-developed friction factor in singly-connected ducts, such as elliptical, polygonal, and isosceles triangular, rectangular, casped, corner ducts, and side ducts; although more comprehensive, this method is also quite complex for implementation and resulted in predictions with an error of ±17%.

Yovanovich and Muzychka [9] developed an approximate expression based on the solution for the elliptical geometry for predicting the Poiseuille number of prismatic domains given by,

$$Po = f \cdot \mathrm{Re}_{\sqrt{A}} = \frac{32\sqrt{\pi}}{0.92^{(\varepsilon-1)}(\sqrt{\varepsilon}-\varepsilon^{1.5})+\varepsilon} \tag{1}$$

where $\sqrt{A}$ is the length scale used for defining Re and ε is the aspect ratio of the channel defined uniquely for different channels. This equation is valid over the range $0.05 \leqslant \varepsilon \leqslant 1$. Muzychka and Yovanovich [10] proposed a new model for predicting the Poiseuille number for fully developed flow in non-circular channels, given by,

$$Po = f \cdot \mathrm{Re}_{\sqrt{A}} = \frac{48}{\sqrt{\varepsilon}\cdot(1+\varepsilon)\left[1-\left(192\frac{\varepsilon}{\pi^5}\right)\tanh\left(\frac{\pi}{2\varepsilon}\right)\right]} \tag{2}$$

Bahrami et al. [11,12] outlined an approximate solution, based on the analytical solution of elliptical ducts, and using the concept of Saint–Venant theorem, for determining the pressure drop of fully developed laminar flow in singly-connected microchannels of arbitrary cross-section. Using a bottom-up approach they showed that the Po is only a function of area of cross-section (A), perimeter (P), and polar moment of inertia (I_p), given by,

$$Po = f \cdot \mathrm{Re}_{\sqrt{A}} = (32\pi^2)\cdot I_p^* \cdot \sqrt{A}/P \tag{3}$$

where the specific polar moment of inertia $I_P^* = I_p/A^2$, and the Reynolds number is based on the square-root of the area of cross-section. They validated the proposed model (with maximum error in the range of 7–9%) with experimental data for rectangular, trapezoidal, and triangular microchannels as well as with numerical results for a variety of shapes. Use of this model requires the location of the centre of the cross-section geometry and the polar moment of inertia about this centre, in addition to the area and the perimeter of cross-section of individual ducts.

Renksizbulut and Niazmand [13] numerically studied simultaneously developing three-dimensional laminar flow in trapezoidal channels. Their numerical methodology was based on transformation of the governing equation into a generalized non-orthogonal coordinate system and the equations were solved using a projection like method. They presented a correlation for predicting fully-developed friction factor as a function of side angle (ϕ) and aspect ratio (ε), given by,

$$Po = 13.9\left(\frac{90^\circ}{\phi}\right)^{-0.07} + (10.4)\exp\left[-(3.25)\cdot\varepsilon\cdot\left(\frac{90^\circ}{\phi}\right)^{0.23}\right] \tag{4}$$

Chakraborty [14] analyzed the flow problem in a straight microchannel of arbitrary cross-section using three general solution methods namely, complex functional analysis, membrane vibration analogy, and variational methods; the usefulness of these

methods were justified through very limited examples and exhaustive testing was not provided. Akbari et al. [15] experimentally studied pressure drop in rectangular microchannels fabricated on poly-dimethyl-siloxane (PDMS). They used their experimental results to independently validate (for the case of rectangular cross-section only) the general model developed by Bahrami et al. [11,12], as noted earlier. Muzychka and Yovanovich [16] presented a detailed review and analysis of the hydrodynamic characteristics of laminar developing as well as fully developed flows in non-circular ducts. Based on scaling analysis they proposed new models for predicting Poiseuille number for developing as well as fully developed flows in non-circular duct geometry. Duan and Yovanovich [17] also reviewed several models for steady laminar flow in long as well as short microchannels of arbitrary shape and aspect ratio.

Tamayol and Baharami [18] had presented an analytical solution for laminar fully-developed flow in hyper-elliptical and regular polygonal cross-sections for predicting the velocity distribution and Poiseuille number. The predicted results were successfully compared with experimental data of other authors for rectangular channels. Kundu et al. [19] have also established an exact analytical solution using separation of variables and approximate analytical techniques such as integral Ritz/Kantorovich method and homotopy perturbation method for fully-developed laminar flow through rectangular channels. Duan and Muzychka [20] studied slip flow in the entrance of circular and parallel plate microchannels by solving a linearized momentum equation. They found that slip flow is less sensitive to analytically-obtained linearized approximations than continuum flow, and the linearization method is an accurate approximation for slip flow. Duan and Muzychka [20] also found that the entrance value of $f\cdot\mathrm{Re}$ is finite and independent of the cross-sectional geometry, but it depends on Kn and tangential momentum accommodation coefficient. Based on the study of slip flow and continuum flow in the hydrodynamic entrance of non-circular microchannels, they proposed a model that can predict $f\cdot\mathrm{Re}$ for developing slip flow and continuum flow in most non-circular microchannels. They also demonstrated that the complete problem may be easily analyzed by combining the asymptotic results for long and short ducts. The effect of duct shape has been minimized by considering the square root of cross-sectional area as the characteristic length scale, and the model is found to be accurate within 10% for most common duct shapes.

Tamayol and Hooman [21] presented closed form solutions for fully developed pressure driven slip-flow in non-circular microchannels. A least-squares-matching of boundary values is employed in the general solution of the Poisson's equation in the cylindrical coordinate, for applying the slip boundary condition at the wall. They analyzed microchannels of three different types of cross sections, i.e., polygonal (with circular section as the limiting case), rectangular and rhombic cross sections, and compared their results successfully with the existing data in the literature.

Recently, Shahsavari et al. [22] presented an analytical solution for velocity and temperature distributions of laminar fully-developed flow of Newtonian, constant property fluids in hyper-elliptical and regular polygonal shaped mini/micro channels subjected to constant axial wall heat flux with uniform peripheral heat flux at a given cross section. The considered geometries cover different shapes such as ellipse, rectangle, rectangle with round corners, rhombus, star-shape, and all regular polygons. They used linear least squares point matching technique to minimize the residual between the actual and the predicted values on the boundary of the channel. Shahsavari et al. [22] predicted hydrodynamic and thermal characteristics of the flow, i.e., pressure drop, local and average Nusselt numbers, and also compared the results for a variety of cross sections with existing solutions from the literature.

A comprehensive review on fluid friction and heat transfer in microchannels is also available in recent work by Muzychka et al. [23]. Most available solutions or methodologies either address only one particular duct shape or are confined to only a limited cross-sectional shapes. Secondly, mostly they are limited to singly-connected ducts only.

In this paper, we present a generalized methodology which can provide local velocity distribution in (a) any arbitrarily shaped singly-connected duct, having at least one plane of angular symmetry, (b) two principal variations of the doubly-connected duct (i) annular duct having an arbitrary outside perimeter while the internal core perimeter is circular, and (ii) annular duct having a circular outside perimeter while the internal core perimeter is arbitrarily shaped. Our approach is based on the extension of the framework proposed by Kolodziej et al. [24]. To the best of our knowledge, such comprehensive treatment of arbitrary shapes has not been reported in open literature. The proposed solution is validated through comparison with some existing theoretical models for a variety of geometries e.g. circular, rectangular, elliptical cross-sections, eccentric circular etc. Additionally, the angular variations of wall shear stress as well as two-dimensional shear stress variations inside the channel are also evaluated for a variety of non-circular channels. Finally we demonstrate the successful application of our methodology to real-time engineering situations.

2. Mathematical formulation

In this work we have analyzed both singly- and doubly-connected ducts. Further, two different variations of doubly-connected ducts have been scrutinized. The domain of present work practically encompasses the entire range of channels and ducts which are routinely employed in different engineering applications with single-phase internal convective flows.

We choose cylindrical coordinate system (r,θ,z) for the mathematical formulation of the problem. The present formulation is generalized in nature and is applicable to any cross-sectional shapes which have at least one plane of symmetry perpendicular to the channel cross-section. Such a situation is only possible when 2π is an integer multiple (N) of the included angle of the cross-sectional segment being considered. Within this symmetric segment, the shape of the channel can be completely arbitrary, as is shown in Fig. 1. The location of channel periphery is described by (r_s,θ), where θ varies from 0 to θ_{sym}. Further, the following assumptions have been made in the formulation:

(a) Flow is adiabatic, single-phase, laminar, fully developed and steady state.
(b) Cross-sectional area is constant in the streamwise direction, z.
(c) Thermo-physical properties of the fluid are constant.
(d) No-slip boundary condition exists everywhere on the duct periphery.
(e) Viscous dissipation is neglected.

Based on the above assumptions the momentum equation in cylindrical coordinate system for the domain considered here is given by:

$$\frac{\partial^2 u}{\partial r^2}+\frac{1}{r}\frac{\partial u}{\partial r}+\frac{1}{r^2}\frac{\partial^2 u}{\partial \theta^2}=\frac{1}{\mu}\frac{dp}{dz} \tag{5}$$

where, $u(r,\theta)$ is the velocity component along the z axis, μ is the dynamic viscosity of fluid, and dp/dz is the driving pressure gradient.

We employ the two-dimensional semi-analytical boundary collocation method, widely used in linear continuous mechanics, to

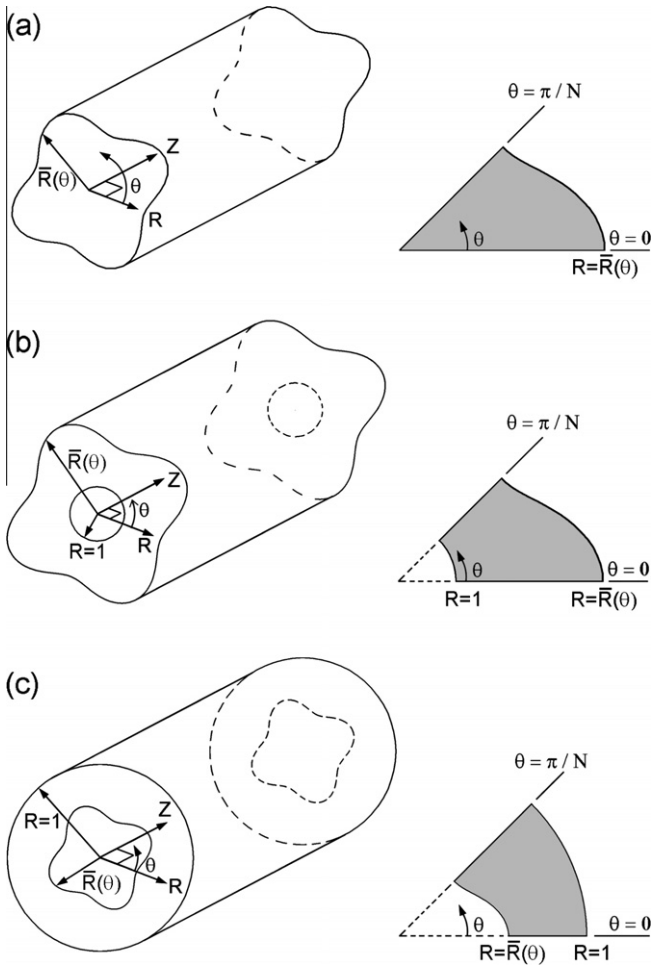

Fig. 1. Three variants of arbitrary shaped duct: (a) Singly-connected duct having arbitrary shaped outer surface and one of its angular symmetric segments. (b) Doubly-connected duct having arbitrary shaped outer surface with an inner circular core and one of its angular symmetric segment. (c) Doubly-connected duct having circular outer surface with an arbitrary shaped inner core and one of its angular symmetric segment.

integrate the above equation. The methodology consists in using the exact solution of the governing differential equation of the problem and satisfying the given boundary conditions only at a finite number of discrete points on the boundary, along with the connectivity conditions at the symmetric planes. In this way, the unknown coefficients of the exact solution can be approximately determined. Such a collocation is needed as one of the boundary conditions is specified at the irregular geometry, as seen in Eq. (6c). Collocation points need to be placed only on the non-circular cross sectional walls (either inner or outer peripheral boundary). Thus, in a singly connected channel, collocation points are considered on the walls of the channel. Secondly, in a doubly connected channel with circular core, collocation points are considered on the outer surface wall. Similarly for a circular channel with non-circular core, collocation points are considered on the inner surface wall only. In this way, the boundary collocation method provides approximate analytical expressions for the solutions through simple numerical calculations, thus making it a semi-analytical method. An extensive review of use of boundary collocation method in linear continuous mechanics is available in [25]. While many applications in the field of continuous mechanics of solid structures have evolved [26], limited applications in solving fluid flow [24,27,28] as well as heat transfer problems [29–32] are also available.

2.1. Singly-connected ducts

Fig. 1(a) depicts a singly-connected duct along with one of its angular symmetric segment ranging from $\theta = 0$ to $\theta = \theta_{sym}$. In this case, the boundary conditions are

$$\partial u/\partial\theta = 0 \quad \text{at} \quad \theta = 0 : \text{symmetry} \tag{6a}$$

$$\partial u/\partial\theta = 0 \quad \text{at} \quad \theta = \theta_{sym} = \pi/N : \text{symmetry} \tag{6b}$$

$$u = 0 \quad \text{at} \quad r = r_s(\theta) : \text{no slip} \tag{6c}$$

Next, we non-dimensionalize the governing equation using the following variables:

$$R = \frac{r}{\ell}, \quad \overline{R} = \frac{r_s}{\ell}, \quad U = \frac{u}{-\frac{\ell^2}{\mu}\frac{dp}{dz}}, \quad \overline{U} = \frac{\bar{u}}{-\frac{\ell^2}{\mu}\frac{dp}{dz}} \tag{7}$$

where, ℓ is the length scale used for non-dimensionalizing and $\bar{u}$ is the average fluid velocity. Different natural length scales are applicable depending on the geometry under consideration; this needs to be fixed *apriori* by inspection. The governing equation in the non-dimensional form will have the form

$$\frac{\partial^2 U}{\partial R^2} + \frac{1}{R}\frac{\partial U}{\partial R} + \frac{1}{R^2}\frac{\partial^2 U}{\partial \theta^2} = -1 \tag{8}$$

The general solution of the above equation is given by [33,34]:

$$\begin{aligned} U(R,\theta) = &-\frac{R^2}{4} + A' + B' \cdot \ln R + C' \cdot \theta + D' \cdot \theta \cdot \ln R \\ &+ \sum_{k=1}^{\infty} (A_k R^{\lambda_k} + B_k R^{-\lambda_k}) \cos(\lambda_k \theta) \\ &+ \sum_{k=1}^{\infty} (C_k R^{\lambda_k} + D_k R^{-\lambda_k}) \sin(\lambda_k \theta) \end{aligned} \tag{9}$$

where, $A', B', C', D', A_k, B_k, C_k, D_k, \lambda_k$ are the unknown coefficients. In the non-dimensional domain, the boundary conditions are:

$$\partial U/\partial\theta = 0 \quad \text{at} \quad \theta = 0 \tag{10a}$$

$$\partial U/\partial\theta = 0 \quad \text{at} \quad \theta = \pi/N \tag{10b}$$

$$U = 0 \quad \text{at} \quad R = \overline{R} \tag{10c}$$

2.1.1. Solution methodology

As the physical domain of the problem is symmetric about the lines $\theta = 0$ and $\theta = \pi/N$ (where N is any integer), Eq. (10a) will be fulfilled if,

$$C' = C_k = D_k = 0 \text{ for } k = 1, 2, 3 \ldots \tag{11}$$

The condition that the flow velocity U is finite at $R = 0$ will be satisfied when,

$$B' = D' = B_k = 0 \tag{12}$$

With these conditions imposed, Eq. (9) will have the form,

$$U(R,\theta) = -\frac{R^2}{4} + A' + \sum_{k=1}^{\infty} (A_k R^{\lambda_k}) \cos(\lambda_k \theta) \tag{13}$$

Eq. (10b) will be fulfilled if

$$\lambda_k = N \cdot k \tag{14}$$

Substituting Eq. (14) in Eq. (13)

$$U(R,\theta) = -\frac{R^2}{4} + A' + \sum_{k=1}^{\infty} (A_k R^{Nk}) \cos(Nk\theta) \tag{15}$$

Introducing new symbols

$$A' = Y_1, A_1 = Y_2, A_2 = Y_3, \text{and so on} \tag{16}$$

$$U(R,\theta) = -\frac{R^2}{4} + Y_1 + \sum_{k=2}^{\infty}[Y_k R^{N(k-1)}]\cos[N(k-1)\theta] \tag{17}$$

where, Y_k are unknown coefficients to be determined so as to get the complete velocity profile given by Eq. (17). Now, from Eq. (10c) and Eq. (17),

$$Y_1 + \sum_{k=2}^{\infty}[Y_k \overline{R}^{N(k-1)}]\cos[N(k-1)\theta] = \overline{R}^2/4 \tag{18}$$

However, the expression given in Eq. (18) cannot be evaluated explicitly due to the unique geometry of the outer periphery having an arbitrary cross-section ($\overline{R}$ is a function of θ). To resolve this issue, a simple/modified boundary collocation method is used wherein a finite number (say M) of equidistant collocation points are considered on the non-circular boundary. The non-circular arbitrary shaped boundary surface is uniquely defined by $\overline{R}(\theta)$ between the limits $\theta = 0$ and $\theta = \pi/N$. Secondly, the infinite series in Eq. (18) is truncated to the first M terms and Eq. (18) is satisfied at the collocation points considered on the non-circular boundary. This results in M number of unknowns (Y_k, $k = 1$ to M) and a matching number of linear equations. Moharana and Das [31,32] had earlier used this technique successfully for heat conduction in a variety of non-circular cross-sectional shapes such as oval, lenticular, teardrop, and eccentric annuli. Now Eq. (18) can then be written as a system of linear equations, with Y_k as the unknown constants, given by,

$$\sum_{k=1}^{M} G_{jk} Y_k = F_j, \quad j = 1,2,3,\ldots,M \tag{19}$$

where,

$$G_{jk} = \overline{R}^{N(k-1)}\cos[N(k-1)\theta] \tag{20}$$

$$F_j = \overline{R}^2/4 \tag{21}$$

The above system of linear equations, represented by Eq. (19), is solved to get the value of the unknown constants, Y_k. This completes the solution procedure of the velocity profile, as given by Eq. (17). The final form of the 'approximate' velocity profile is then given by,

$$U(R,\theta) = -\frac{R^2}{4} + Y_1 + \sum_{k=2}^{M}[Y_k R^{N(k-1)}]\cos[N(k-1)\theta] \tag{22}$$

It may be noted that the number of points to be taken on the boundary for arriving at a reasonably accurate solution depends on the complexity of the arbitrary shape, although the absolute accuracy of the solution is not a monotonic function of the number of points chosen. We will come back to this issue in a later section after discussing the various test cases. As will be noted, the solutions obtained by this technique are sufficiently accurate for engineering estimations.

2.2. Doubly-connected duct

For doubly-connected ducts of arbitrary cross-sectional shapes, we consider two cases here, (a) Arbitrary cross-section duct having a circular core inside the duct situated at the origin of the coordinate system, (b) Circular cross-section duct having an arbitrary shaped core inside the duct situated at the centre of the coordinate system. In both these cases, the fluid flow takes place in the annular space, as shown in Fig. 1(b) and (c).

2.2.1. Arbitrarily shaped duct with a circular core

A doubly-connected arbitrary cross-section duct having a circular core at the origin of the cylindrical coordinate system, and one of its symmetric segment are shown in Fig. 1(b). The non-dimensional variables considered for this geometry are as follows:

$$R = r/r_i, \quad \overline{R} = r_s/r_i \tag{23}$$

such that for this geometric configuration, $1 \leqslant R \leqslant \bar{R}$. The boundary conditions in non-dimensional form are as follows:

$$\partial U/\partial\theta = 0 \quad \text{for} \quad \theta = 0 \tag{24a}$$

$$\partial U/\partial\theta = 0 \quad \text{for} \quad \theta = \pi/N \tag{24b}$$

$$U = 0 \quad \text{for} \quad R = 1 \tag{24c}$$

$$U = 0 \quad \text{for} \quad R = \overline{R} \tag{24d}$$

Considering the same approach as discussed in Section 2.1.1 for a singly-connected duct, the velocity profile in the domain of the symmetric segment will be,

$$U(R,\theta) = -\frac{1}{4}(R^2-1) + Y_1 \ln R + \sum_{k=2}^{\infty} Y_k (R^{N(k-1)} - R^{-N(k-1)}) \times \cos[N(k-1)\theta] \tag{25}$$

where Y_k are the unknown coefficients. The corresponding set of linear equations from which one need to find the unknown coefficients Y_k will be

$$Y_1 \ln \overline{R} + \sum_{k=2}^{\infty} Y_k (\overline{R}^{N(k-1)} - \overline{R}^{-N(k-1)})\cos[N(k-1)\theta] = \frac{1}{4}(\overline{R}^2 - 1) \tag{26}$$

2.2.2. Circular duct with an arbitrarily shaped core

A doubly-connected circular cross-section duct having an arbitrary shaped core at the origin of the cylindrical coordinate system and one of its symmetric segment are shown in Fig. 1(c). The non-dimensional variables considered for this geometry are as follows:

$$R = r/r_o, \quad \overline{R} = r_s/r_o \tag{27}$$

such that for this geometric configuration, $\bar{R} \leqslant R \leqslant 1$. The boundary conditions in non-dimensional form are as follows,

$$\partial U/\partial\theta = 0 \quad \text{at} \quad \theta = 0 \tag{28a}$$

$$\partial U/\partial\theta = 0 \quad \text{at} \quad \theta = \pi/N \tag{28b}$$

$$U = 0 \quad \text{at} \quad R = 1 \tag{28c}$$

$$U = 0 \quad \text{at} \quad R = \overline{R} \tag{28d}$$

Considering the same approach as discussed in Section 2.1.1 for a singly-connected duct, the velocity profile in the domain of the symmetric segment will be,

$$U(R,\theta) = -\frac{1}{4}(R^2-1) + Y_1 \ln R + \sum_{k=2}^{\infty} Y_k (R^{N(k-1)} - R^{-N(k-1)}) \times \cos[N(k-1)\theta] \tag{29}$$

where Y_k are the unknown coefficients. The corresponding set of linear equations from which one need to find the unknown coefficients Y_k will be,

$$Y_1 \ln \overline{R} + \sum_{k=2}^{\infty} Y_k (\overline{R}^{N(k-1)} - \overline{R}^{-N(k-1)})\cos[N(k-1)\theta] = \frac{1}{4}(\overline{R}^2 - 1) \tag{30}$$

3. Estimation of transport coefficients

Estimation of the momentum flux transport inside the arbitrarily shaped ducts, represented by Poiseuille number, is the fundamental quantity of interest and is defined as,

$$Po = f \cdot \mathrm{Re}_L = \frac{2}{\bar{U}}\left(\frac{L}{\ell}\right)^2 = \frac{2\bar{L}^2\bar{A}}{I} \tag{31}$$

where, $\bar{U}$ is the dimensionless average fluid velocity, I is the integration term for calculating the average fluid velocity, $\bar{A}$ is the dimensionless area of cross-section of the channel, and $\bar{L}$ is the ratio of L and ℓ. L is the characteristic length scale used to define the Reynolds number. The calculation of average fluid velocity $\bar{U}$ and the expression for I are detailed in the Appendix A. Darcy–Weisbach factor f and Re are given respectively by,

$$f = -\left(\frac{2D_h}{\rho\bar{u}^2}\right)\left(\frac{dp}{dz}\right) \tag{32}$$

$$\mathrm{Re}_L = \rho \cdot \bar{u} \cdot L/\mu \tag{33}$$

The three components of the shear stress acting at any point in the cylindrical coordinates are given by,

$$\tau_{r\theta} = \mu\left[r\frac{\partial}{\partial r}\left(\frac{u_\theta}{r}\right) + \frac{1}{r}\frac{\partial u_r}{\partial \theta}\right] \tag{34a}$$

$$\tau_{rz} = \mu\left[\frac{\partial u_r}{\partial z} + \frac{\partial u_z}{\partial r}\right] \tag{34b}$$

$$\tau_{\theta z} = \mu\left[\frac{\partial u_\theta}{\partial z} + \frac{1}{r}\frac{\partial u_z}{\partial \theta}\right] \tag{34c}$$

In the present case, the radial velocity (u_r) as well as the angular velocity (u_θ) of fluid is zero. Thus,

$$\tau_{r\theta} = 0, \quad \tau_{rz} = \mu\frac{\partial u_z}{\partial r}, \quad \tau_{\theta z} = \frac{\mu}{r}\frac{\partial u_z}{\partial \theta} \tag{35}$$

So the shear stress at any point is given by

$$\tau = \sqrt{(\tau_{rz})^2 + (\tau_{\theta z})^2} \tag{36}$$

In dimensionless form the two shear stress components will be

$$\bar{\tau}_{\theta z} = -\sum_{k=2}^{\infty} N(k-1)\left[Y_k R^{N(k-1)}\right]\sin\left[N(k-1)\theta\right] \tag{37}$$

$$\bar{\tau}_{rz} = \frac{R}{2} - \sum_{k=2}^{\infty} N(k-1)\left[Y_k R^{N(k-1)-1}\right]\cos\left[N(k-1)\theta\right] \tag{38}$$

For shear stress along the wall(s) of any channel, $R = \bar{R}$.

4. Results and discussion

In this section, the applicability of the present scheme is demonstrated by considering various complicated singly-as well as doubly-connected geometries. It is noted that many standard/regular shapes (such as circular, square, rectangular etc.), for which analytical solutions are available, are indeed the sub-sets of the complicated shapes considered here. Thus, the results obtained by the present study are first benchmarked against standard geometries. Subsequently, complicated geometries are considered and their transport parameters are presented. Finally, an actual microchannel shape, as obtained by standard micromachining technique for which experimental data are available [35], is chosen for comparison. While this shape is close to trapezoidal, it is very difficult to achieve regular geometries and sharp corner vertices; thus, no analytical solution for such an 'irregular' real-time shape is available. It is demonstrated how the present solution can accurately predict the friction factor of the channel, without assuming it to be a regular trapezoid and treating it as an arbitrarily shaped duct. As will be noted, there is considerable improvement in the actual prediction of the pressure drop by the application of the present technique.

4.1. Singly-connected duct

For the purpose of validation of Eq. (22) describing the velocity profile, an elliptical cross-sectioned duct with aspect ratio ($\varepsilon = a/b$, where a, and b are semi-major and semi-minor axes, respectively) equal to 1.5 is considered. The analytical solution for the dimensionless velocity profile of an elliptical duct is given by [36],

$$U = \frac{\varepsilon^2}{2(\varepsilon^2+1)}\left[1 - \left(\frac{R\cos\theta}{\varepsilon}\right)^2 - (R\sin\theta)^2\right] \tag{39}$$

Fig. 2(a) shows the comparison of radial variation of dimensionless velocity U at different angular positions inside the duct of elliptical cross-section. From Fig. 2(a), it is clear that the predicted velocity is in excellent agreement with the analytical solution [36]. Secondly, the comparison of the velocity profile for a rectangular channel with the analytical solution [37] and the semi-analytical solution of Spiga and Morini [38] is shown in Fig. 2(b) which depicts the radial variation of dimensionless velocity U along the radial lines AB, AC, and AD (see inset of Fig. 2(b)). Next, we predict the velocity contours in a trapezoidal channel, having top and bottom width equal to $2a$ and $2b$, respectively, the height of the channel being h, as shown in Fig. 3(a). This is a commonly used shape in micro-channel applications. Also, as noted earlier, various standard shapes such as rectangular and square cross-sections, can be easily obtained from this generic trapezoidal shape. Similarly other frequently used channels for heat transfer applications such as (i) semi-elliptical or lenticular (which consists of a semi-circular and a semi-elliptical duct joined together where a, and b are semi-major axis, and semi-minor axis of the elliptical portion respectively; the circular portion has radius equal to b), (ii) lens shaped (combination of two circular arcs, each with radius r, subtending an angle of 2θ at its centre), (iii) U-shaped, (iv) continuous corrugated wall (for example, with sinusoidal curves), (v) discontinuous corrugated wall, etc., can also be easily analyzed, as shown in Fig. 3(b)–(f), respectively. Some other shapes, such as moon crescent shaped, n-sided regular polygon, and star shaped, were also solved but not reported here.

Next, after validating the velocity profiles for some shapes for which analytical or semi-analytical solution is available and generating velocity profiles for more complicated and generic shapes, we focus our attention on shear stress calculation. Begum and Zamir [39] have presented a correlation for wall shear stress distribution in an elliptical duct, given in the non-dimensional form as,

$$\bar{\tau}_w = \bar{R}\left(\frac{\varepsilon^2}{1+\varepsilon^2}\right)\sqrt{\left(\frac{\cos^2\theta}{\varepsilon^4}\right) + sin^2\theta} \tag{40}$$

We compare this with the results obtained by the present analysis (from Eq. (36)–(38)) for the purpose of validating the scheme, as shown in Fig. 4(a), which shows the angular variation of dimensionless wall shear stress in an elliptical duct as a function of the duct aspect ratio. For circular tubes (elliptical tube with aspect ratio 1) the non-dimensional wall shear stress equals to 0.25 [40] and is constant in the angular direction, as highlighted in Fig. 4(a). With increasing aspect ratio, the angular variation gradually deviates from uniform distribution; being minimum at the ends of major axis and maximum at the ends of minor axis. Secondly, the higher the aspect ratio, the higher is the deviation from the uniform value

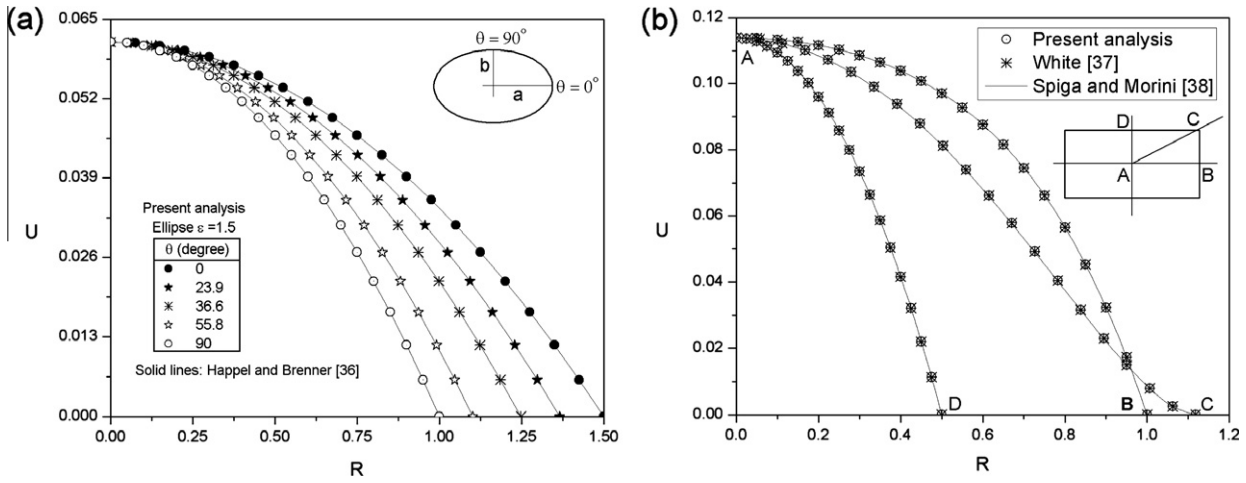

Fig. 2. Radial variation of dimensionless velocity U at different angular positions in (a) an elliptic duct with an aspect ratio $a/b = 1.5$ (b) rectangular duct with an aspect ratio of 2.0.

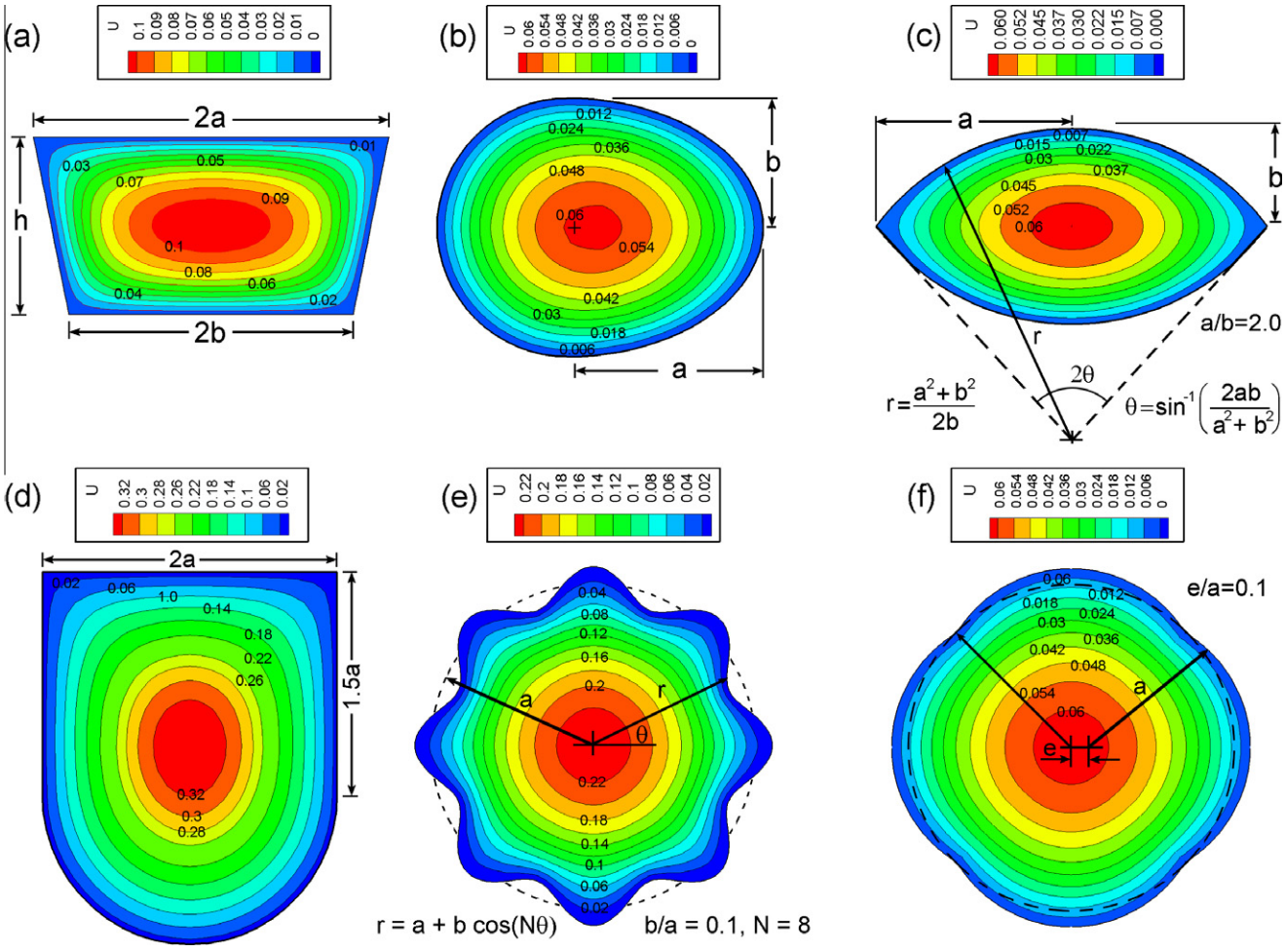

Fig. 3. Velocity contour in different shaped singly-connected ducts (a) trapezoidal (b) semi-elliptical duct with $a/b = 1.5$ (c) Lens shaped (d) U shaped channel (e) continuous corrugated (f) discontinuous corrugated.

of 0.25. From Fig. 4(a) it is clear that the prediction of the wall shear using present analysis matches perfectly with that of Begum and Zamir [39] as well as Kundu and Cohen [40]. Fig. 4(b) depicts the angular variation of dimensionless wall shear distribution in a semi-elliptic duct (half elliptical and half circular). The dotted line represent the shear stress distribution had the tube either full elliptical or circular. Fig. 4(c) depicts the angular variation of dimensionless wall shear distribution in a lens shaped duct. For $a = b$ the lens shaped duct will tend to a circular tube. Thus, the wall shear stress distribution at $a/b = 1$ comes out to be equal to

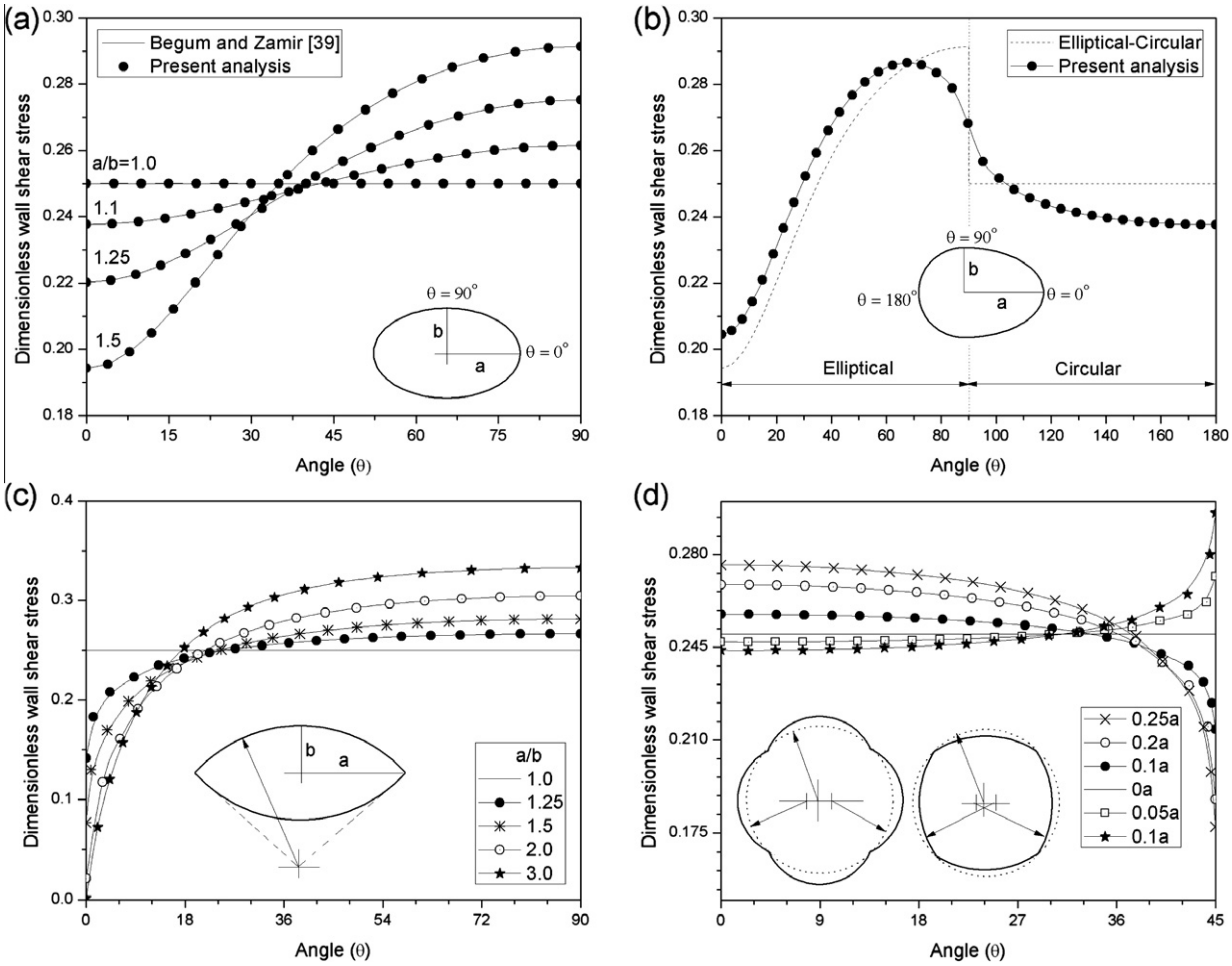

Fig. 4. Angular variation of dimensionless wall shear stress as a function of aspect ratio in different shaped singly-connected ducts (a) elliptical (b) semi-elliptical (c) lens shaped (d) discontinuous corrugated.

0.25 as discussed above and also shown in Fig. 4(c). With increasing aspect ratio, the shear stress distribution deviates from uniformity; tending towards zero at the intersection of two circular arcs, i.e. at $\theta = 0°$, and maximum at the flat point of the circular arc i.e. at $\theta = 90°$. Fig. 4(d) depicts the angular variation of dimensionless wall shear distribution in two different discontinuous corrugated walled ducts as shown in the inset figure.

4.2. Doubly-connected duct

After analyzing the singly-connected ducts of arbitrary shapes, we take up the doubly-connected cases; two principal variations of which are: (i) annular duct having an arbitrary outside perimeter while the internal core perimeter is circular (refer Fig. 1(b)), and (ii) annular duct having a circular outside perimeter while the internal core perimeter is arbitrarily shaped (refer Fig. 1(c)). Generalized analytical solutions of fully-developed velocity profiles are not available for such doubly-connected ducts. However, limited number of doubly-connected ducts has been analyzed which we will make use of for validation.

Fig. 5 shows a comparison of dimensionless fluid velocity profile along the radial direction at $\theta = 0$ (see the inset figure) in an annular elliptical duct having a circular core at the centre of the duct for $\varepsilon = a/b = 1.25$ and 2.0. It is clear that the prediction of the velocity profile using present boundary collocation method is in perfect agreement with the semi-analytical solution, as given by Shivakumar [41].

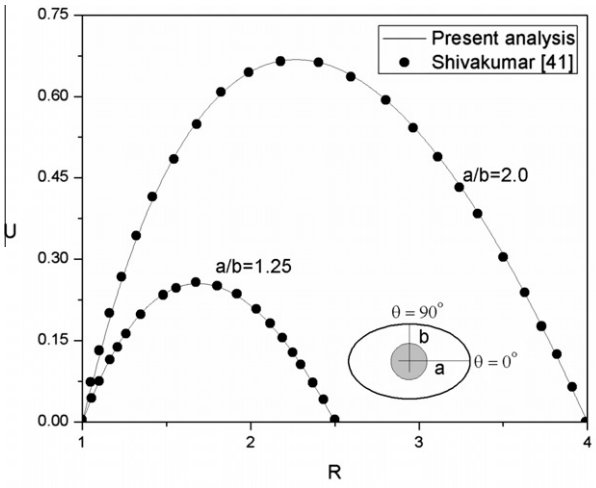

Fig. 5. Dimensionless velocity of the fluid in the radial direction, along the semi-major axis, in a doubly-connected elliptical duct, having a concentric circular core.

Fig. 6(a) shows the velocity profile corresponding to $e/r_i = 1$ and $r_o/r_i = 3.0$, and Fig. 6(b) shows the variation of Poiseuille number with the geometry, for an eccentric annulus formed by two circular sections of radii r_i and r_o, and having an eccentricity, e. The predictions of *Po* as a function of these geometrical parameters using the

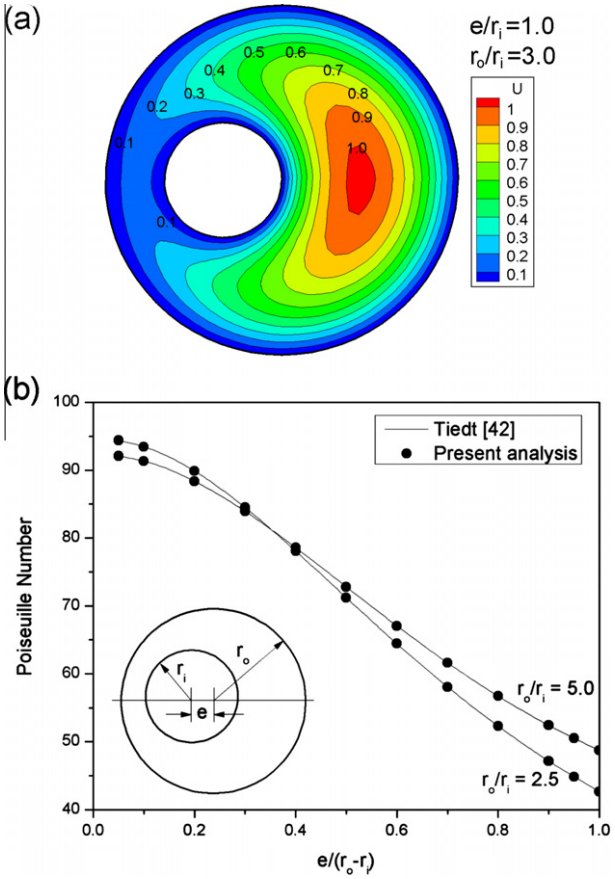

Fig. 6. (a) Velocity contours and, (b) Poiseuille number, for an eccentric duct as a function of its geometrical parameters.

present boundary collocation method are in perfect agreement with that of Tiedt [42], as reported by Shah and London [4]. The length scale used for calculating the Reynolds number here is $L = 2(r_o - r_i)$.

Fig. 7 presents the velocity contour in different doubly-connected annular ducts having outside perimeters corresponding to (a) an ellipse (b) a semi-elliptic (c) *U*-shaped, and (d) Square cross-sections. For all these shapes, the internal core is circular in cross-section and is placed eccentrically, as shown in Fig. 7(a)–(d). The location of the maximum velocity in the cross-section is related to the direction of imposed eccentricity of the inner core.

Fig. 8 presents velocity contour in three examples of the second variation of doubly-connected annular ducts, i.e., having a circular outer perimeter and the following shaped inner core (a) concentric elliptic core (b) concentric rectangular shaped core with semi-circular ends, and (c) lenticular shaped core having an eccentricity, *e*. It is clear that prediction of fully-developed velocity profiles in such complicated shapes can be easily handled by the boundary collocation methodology, as presented here.

4.3. Comparison with experimental test case

In the previous section, a variety of singly- and doubly-connected duct shapes were analyzed. In this section, we highlight an application of the present methodology in accurately predicting the fully developed velocity profile, and therefore the net pressure drop, inside a microchannel which has been fabricated by etching process on a silicon substrate [35]. It is to be noted that most micro-fabrication techniques will normally not produce mathematically well-defined or ideal geometries. For example, it is impossible to get a sharp cornered channel by laser micromachining or by chemical etching process. Some finite corner radii will always remain. For predicting pressure-drop or for validating the experiments, many investigators tend to use correlations which are typically developed for standard ideal well-defined geometries, which are closest to the actual profile of the channel cross-section. Frequently, this provides inaccurate basis for comparison and therefore the predictions are not satisfactory.

Steinke and Kandlikar [35] studied single-phase liquid friction factor in microchannels. The dimensions were first measured by non-destructive optical measurement technique. It was reported that the microchannel has a rectangular cross-section having dimensions 201 ± 5 μm and 247 ± 5 μm, see Fig 9(a). After the fluid-flow experiment, the test section was cleaved for better estimation of the channel dimensions. The improved cross-section profile of the channel which was first considered be a rectangle was actually found to be as shown in Fig. 9(b). As the next step towards improving the prediction of transport parameters, Steinke and Kandlikar [35] used the trapezoidal shape, as shown in Fig. 9(c). This was done as no analytical solution is available for treating the arbitrary shape of Fig. 9(b), as obtained by the etching process. However, the present collocation technique can easily and accurately handle the geometry exactly as in Fig. 9(b), in its true shape as obtained by the manufacturing process and there is no need for using 'closest regular/ideal geometry' approximation. The friction factor values for all the three shapes shown in Fig. 9(a)–(c) are predicted using the present collocation technique and presented in Table 1. The friction factor values predicted for the rectangular (Fig. 9(a)) as well as the trapezoidal (Fig. 9(c)) channel using Muzychka and Yovanovich [10] are also given in Table 1 for a direct comparison.

Steinke and Kandlikar [35] revised the friction factor values after cleaving the channel cross-section to be $Po = 58$ where as the best estimated friction factor value of this actual shape (Fig. 9(b)) is found to be 65.2, using the present collocation technique. The increase in the friction factor value is due to the round corners and decrease in area of cross-section of the actual channel (Fig. 9(b)) as compared to the assumed trapezoidal channel (Fig. 9(c)). Similar phenomenon was also reported by Shah [7], where an equilateral triangular duct with and without round corners at the apex was analyzed. For a sharp angled equilateral triangular duct, the *Po* comes out to be 53.34. Rounding off of the corners increases the *Po*; when all the three corners of the equilateral triangular duct are rounded-off, the *Po* increases to 63.97. This was also independently confirmed by the present method.

4.4. Role of collocation points

The maximum error in the boundary collocation method is a function of number of collocation points as well as the co-ordinates of collocation points [43]. If the number of collocation points is less, the accuracy of the solution may be unsatisfactory; on the other hand, more number of collocation points may lead to ill-conditioned system of the linear equations from which the unknown coefficients Y_k are determined. Sometimes, error occurs in satisfying the boundary conditions between the collocation points despite the fact that at the collocation points themselves, the conditions are fulfilled exactly. The above difficulty can be avoided by using some adaptive versions of the boundary collocation method. Two such versions are proposed by Kolodziej and Starosta [43] for solving two-dimensional Laplace equation satisfying the maximum error principle. Kolodziej and Starosta [43] observed the behavior of maximum local error as a function of number of collocation points. They found that for equidistant collocation points, local error monotonically decreases with the increase of the number of collocation points. However, beyond a certain number of

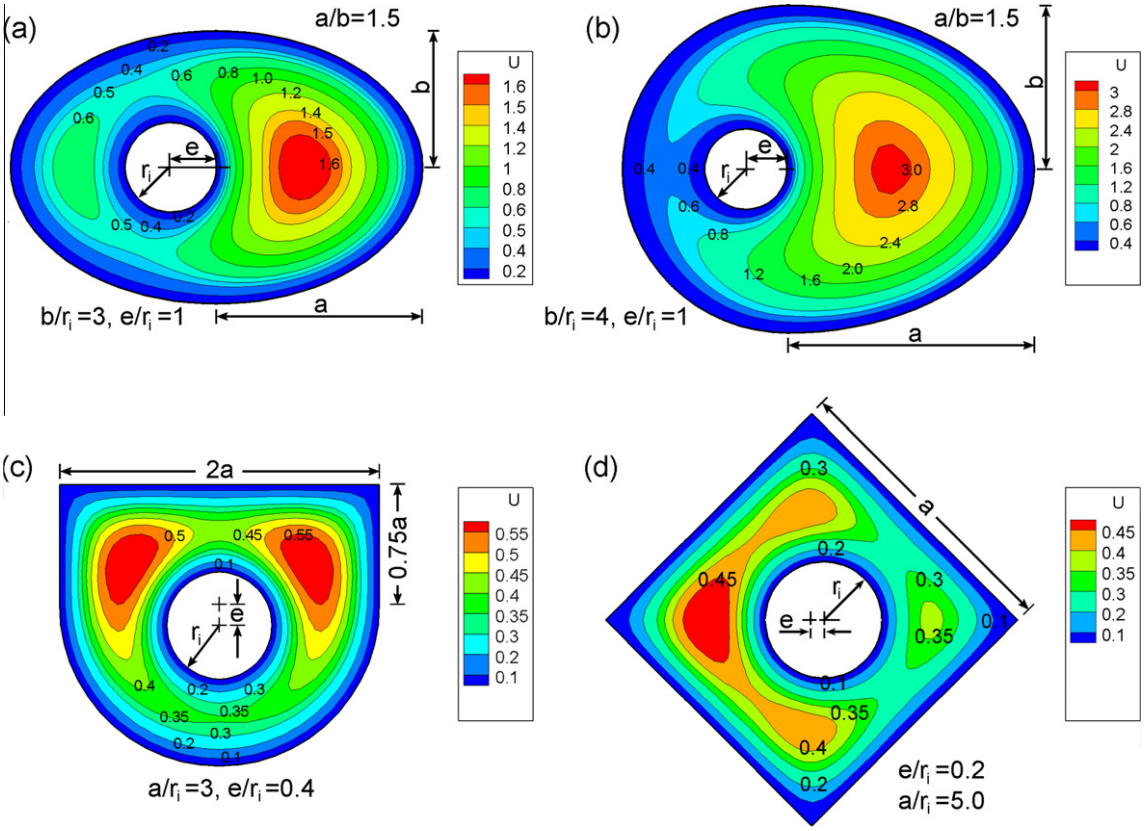

Fig. 7. Velocity contours in different shaped doubly-connected ducts having an eccentric circular inner core (a) elliptic duct (b) semi-elliptic duct (c) *U*-shaped duct (d) square duct.

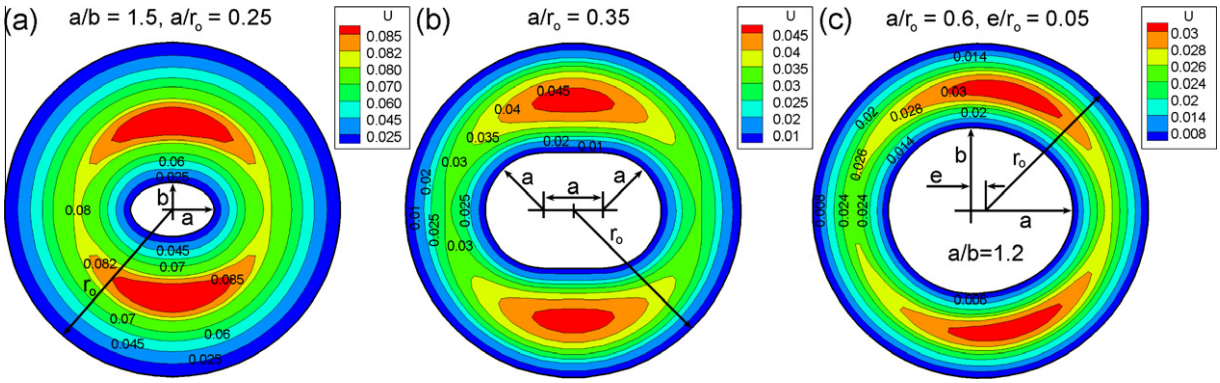

Fig. 8. Velocity contours in doubly-connected annular ducts having a circular outer perimeter and with the following inner core shapes (a) concentric elliptic (b) concentric rectangular shaped with semi-circular ends (c) semi-elliptical (lenticular) shaped placed eccentrically.

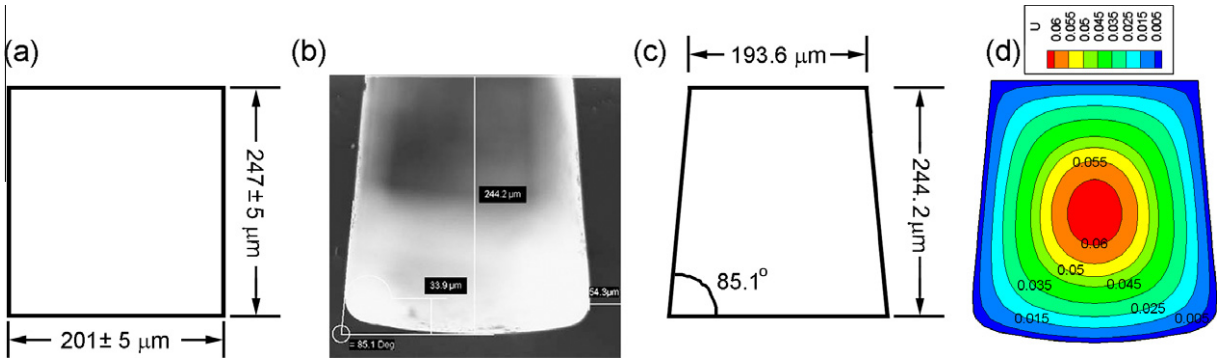

Fig. 9. (a) Rectangular microchannel with the dimensions resulting from the optical measurement technique (b) the actual channel cross-section after it is cleaved (c) the channel cross-section considered by Steinke and Kandlikar [35] for recalculation (d) the velocity contour of the actual microchannel cross-section predicted using the boundary collocation method.

collocation points, ill-conditioning may occur, wherein the error increases and/or oscillates. The reason for this behavior is the worsening of the conditioning of equation sets with increasing number of collocation points. The present analysis is based on the adaptive version, as suggested by Kolodziej and Starosta [43].

Fig. 10(a) shows the effect of number of collocation points in predicting the radial variation of dimensionless velocity U, for a liquid flowing inside a rectangular channel (aspect ratio of 0.5), at three angular positions along the radial lines AB, AC, and AD. This problem is symmetric about $\theta = 0$ (along AB) and $\theta = \pi/2$ (along AD), thereby requiring the placement of collocation points along B–C–D at equal distance intervals, as has been clarified in the inset of Fig. 10(b). Apparently, as seen in Fig. 10(a), the number of collocation points does not have a major impact on this problem. However, minute observation of the change in peak velocity, with respect to the number of collocation points, depicted in Fig. 10(b), does show the effect of increasing the number of points. Fig. 10(b) shows the percentage difference between the predicted values of U at the centre of the rectangular tube (i.e. U_{max}) by choosing different number of collocation points, from 9 to 61, the basis being the maximum velocity at the largest number of collocation points, i.e. 61. The error is rather small, amounting to a maximum of 0.0024% only for the number of collocation points equal to 9.

Fig. 11(a) shows the effect of number of collocation points in predicting the value of Poiseuille number in a square duct. For a square duct $Po = 56.90832$ [4], which is shown as the horizontal line in Fig. 11(a). This problem is symmetric about $\theta = 0$ (along AB) and $\theta = \pi/4$ (along AC) (see inset in Fig. 11(a)). So, this requires placing collocation points along B–C at equal distance intervals. This is demonstrated in Fig. 11(a). From Fig. 11(a) it can be seen

Table 1
Poiseuille Number for different channel shapes as in Fig. 9, based on $L = D_h$.

Results by	Poiseuille number		
	Rectangular (Fig. 9(a))	Actual shape (Fig. 9(b))	Trapezoidal (Fig. 9(c))
Present technique	57.44	65.2	57.06
Muzychka and Yovanovich [10]	57.20	–	56.70
Steinke and Kandlikar [35]	–	–	58.0

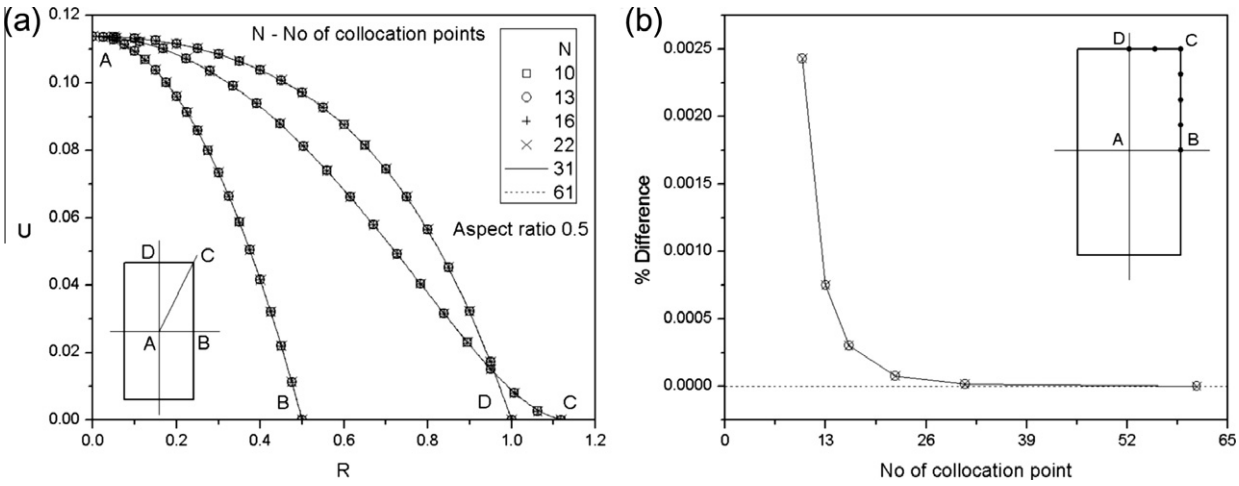

Fig. 10. (a) Velocity profile in a rectangular duct as a function of number of collocation points (b) Corresponding error in the peak velocity (with respect to that obtained for 61 collocation points), as a function of number of collocation points.

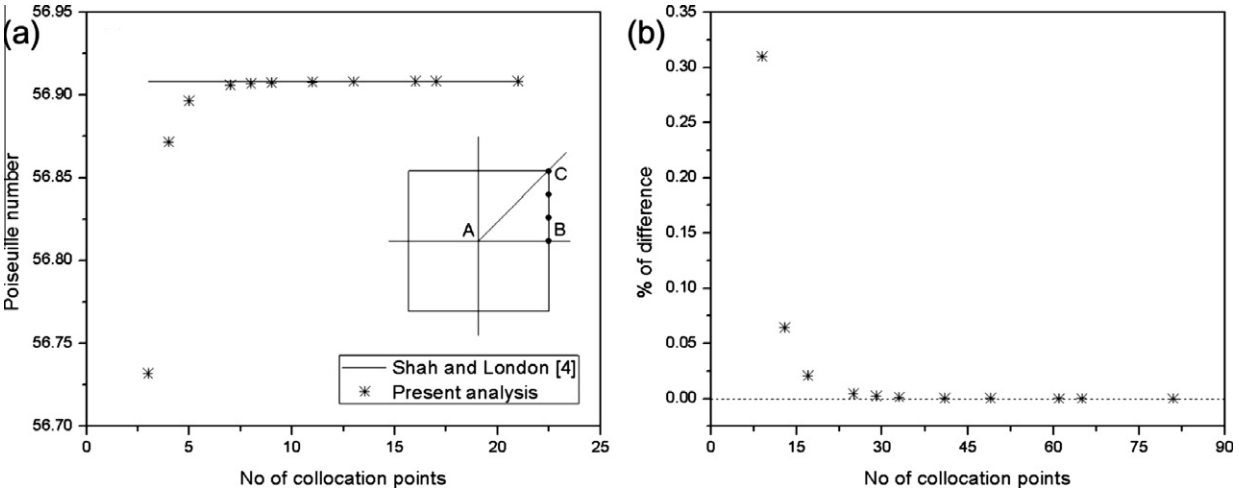

Fig. 11. (a) Comparison of Po for a square duct as a function of number of collocation points chosen for obtaining the solution (b) The corresponding percentage difference between the Po values predicted using present analysis and that provided by Shan and London [4].

that there is not much difference between predicted values for different number of collocation points. To observe this minor difference in a magnified form, Fig. 11(b) presents percentage difference between the value of *Po* as given by Shah and London [4] and predicted values using different number of collocation points (here minimum 3 to maximum 21). The maximum difference observed at the minimum number of collocation points used (i.e. 3) is 0.31% only.

It is also observed that lesser number of collocation points is required for achieving accurate results for the geometries with smaller variation of r_s in the angular direction. For example, low aspect ratio elliptical duct will require less number of collocation points and the predictions are highly accurate. Also, the chances of getting an ill-conditioned solution reduce with increasing number of collocation points.

5. Summary and conclusions

A two-dimensional boundary collocation method is used for the analysis of laminar fully developed internal fluid flow through a channel of arbitrary cross-section. It is demonstrated that fully developed velocity profiles can be effectively predicted by this technique for practically any singly- or doubly-connected duct of arbitrary cross-section having at least one plane of even angular symmetry. Hence, the shear stress and friction factor can be accurately estimated. Validation of the technique has been done against available analytical/semi-analytical results available for standard geometries. A gamut of complex shapes, practically covering the entire range of possible engineering applications, has been analyzed by this collocation technique. It is concluded that this methodology is particularly suitable for analyzing practical microchannel applications wherein it is impossible to obtain regular or standard cross-sectional geometries and/or sharp angled vertices by available micro-machining routes. The efficacy of the collocation technique in handling such situations has been demonstrated.

Acknowledgement

The work is funded by the Department of Science and Technology, Government of India, under the sponsored project No: DST/CHE/20060304 titled 'Micro-devices for process applications'.

Appendix A.

The average velocity of fluid over the whole area of cross-section of any duct is defined as,

$$\bar{u} = \frac{1}{A}\int_A u \cdot dA \tag{A.1}$$

The average velocity in dimensionless form will be,

$$\overline{U} = \frac{1}{\overline{A}}\int_A U \cdot R \cdot dR \cdot d\theta = \frac{I}{\overline{A}} \tag{A.2}$$

where, the integration I is given separately for singly- and doubly-connected ducts as follows,

A.1. Singly-connected duct

For a singly-connected duct, using the expression for the velocity profile as given in Eq. (22),

$$I = 2N\int_0^{\pi/N}\left(-\frac{\overline{R}^4}{16} + \sum_{k=1}^{M}\frac{\left[Y_k\overline{R}^{N(k-1)+2}\right]\cos\left[N(k-1)\theta\right]}{N(k-1)+2}\right)d\theta \tag{A.3}$$

A.2. Doubly-connected duct

For a doubly-connected duct, using the expression for the velocity profile as given in Eq. (25) or Eq. (29),

$$I = 2N\int_0^{\pi/N}\left(\begin{array}{l}\left(\frac{\overline{R}^2}{8}-\frac{\overline{R}^4}{16}-\frac{1}{16}\right)+Y_1\left(\frac{\overline{R}^2}{2}\left(\ln\overline{R}-\frac{1}{2}\right)+\frac{1}{4}\right)\\ +\sum_{k=2}^{M}Y_k\left[\frac{\overline{R}^{N(k-1)+2}}{N(k-1)+2}+\frac{\overline{R}^{-N(k-1)+2}}{N(k-1)-2}-\left(\frac{2N(k-1)}{N^2(k-1)^2-4}\right)\right]\cos[N(k-1)\theta]\end{array}\right)d\theta \tag{A.4}$$

In the present work the above integrations are carried out numerically using simpsons 3/8 rule.

References

[1] P.N. Rao, D. Kunzru, Fabrication of microchannels on stainless steel by wet chemical etching, J. Micromech. Microengrg. 17 (2007) 99–106.
[2] S.J.J. Lee, N. Sundararajan, Microfabrication for Microfluidics, Artech House, Boston, 2010.
[3] D. Li (Ed.), Encyclopedia of Microfluidics and Nanofluidics, Springer, 2008.
[4] R.K. Shah, A.L. London, Laminar Flow Forced Convection in Ducts, Supplement 1 to Advances in Heat Transfer, Academic press, New York, 1978.
[5] S. Kakaç, R.K. Shah, A.E. Bergles, Low Reynolds Number Flow Heat Exchangers, Springer, 1983.
[6] S. Kakaç, R.K. Shah, W. Aung, (Eds.), Handbook of Single-phase Convective Heat Transfer, John Wiley & Sons, New York, USA, 1987.
[7] R.K. Shah, Laminar flow friction and forced convection heat transfer in ducts of arbitrary geometry, Int. J. Heat Mass Transfer 18 (1975) 849–862.
[8] T. Yilmaz, General equations for pressure drop for laminar flow in ducts of arbitrary cross-sections, J. Energy Res. Technol. 112 (1990) 220–223.
[9] M.M. Yovanovich, Y.S. Muzychka, Solutions of Poission equation within singly- and doubly-connected prismatic domains, in: Proceedings of National Heat Transfer Conference, Baltimore, MD, 1997.
[10] Y.S. Muzychka, M.M. Yovanovich, Laminar flow friction and heat transfer in non-circular ducts and channels: Part I – Hydrodynamic problem, Compact heat exchangers: A Festschrift on the 60th Birthday of Ramesh K. Shah, Grenoble, France, 2002.
[11] M. Bahami, M.M. Yovanovich, J.R. Culham, Pressure drop of fully-developed, laminar flow in microchannels of arbitrary cross-section, J. Fluids Engrg. 128 (2006) 1036–1044.
[12] M. Bahrami, M.M. Yovanovich, J.R. Culham, A novel solution for pressure drop in singly-connected microchannels of arbitrary cross-section, Int. J. Heat Mass Transfer 50 (2007) 2492–2502.
[13] M. Renksizbulut, H. Niazmand, Laminar flow and heat transfer in the entrance region of trapezoidal channels with constant wall temperature, J. Heat Transfer 128 (2006) 63–74.
[14] G. Chakraborty, A note on methods for analysis of flow through microchannels, Int. J. Heat Mass Transfer 51 (2008) 4583–4588.
[15] M. Akbari, D. Sinton, M. Bahrami, Pressure drop in rectangular microchannels as compared with theory based on arbitrary cross-section, J. Fluids Engrg. 131 (2009). pp. 041202-1-8.
[16] Y.S. Muzychka, M.M. Yovanovich, Pressure drop in laminar developing flow in noncircular ducts: a scaling and modeling approach, J. Fluids Engrg. 131 (2009). pp. 111105-1-11.
[17] Z. Duan, M.M. Yovanovich, Pressure drop for laminar flow in microchannels of arbitrary cross-sections, in: Proceedings of 25th IEEE Semiconductor Thermal Measurement and Management Symposium, IEEE, San Jose, USA, 2009.
[18] A. Tamayol, M. Bahrami, Laminar flow in microchannels with noncircular cross-section, J. Fluids Engrg. 132 (2010). pp. 111201-1-9.
[19] B. Kundu, S. Simlandi, P.K. Das, Analytical techniques for analysis of fully developed laminar flow through rectangular channels, Heat Mass Transfer 47 (2011) 1289–1299.
[20] Z. Duan, Y.S. Muzychka, Slip flow in the hydrodynamic entrance region of circular and noncircular microchannels, J. Fluids Engrg. 132 (2010). pp. 011201(1-13).
[21] A. Tamayol, K. Hooman, Slip-flow in microchannels of non-circular cross sections, J. Fluids Engrg. 133 (2011) 1–8. pp. 091202(1–8).
[22] S. Shahsavari, A. Tamayol, E. Kjeang, M. Bahrami, Convective heat transfer in microchannels of noncircular cross sections: an analytical approach, J. Heat Transfer 134 (2012). pp. 091701(1–10).
[23] Y.S. Muzychka, Z.P. Duan, M.M. Yovanovich, Fluid friction and heat transfer in microchannels, in: S.K. Mitra, S. Chakraborty (Eds.), Microfluidics and Nanofluidics Handbook: Chemistry, Physics, and Life Science Principles, CRC Press, Boca Raton, USA, 2012.
[24] J.A. Kolodziej, A. Uscilowska, M. Cialkowski, Semi-analytical approximations of the laminar friction coefficients for flow in conduits with polygonal cross-section, Acta Mech. 158 (2002) 127–144.
[25] J.A. Kolodziej, Review of application of boundary collocation method in mechanics of continuous media, Solid Mech. Arch. 12 (1987) 187–231.
[26] J.A. Kolodziej, A.P. Zielinski, Boundary Collocation Techniques and their Application in Engineering, WIT Press, Southampton, Boston, 2009.

[27] A. Kucaba-Piêtal, Application of boundary collocation method in fluid mechanics, in: Second Conference on Numerical Analysis and Applications, University of Rousse, Rousse, Bulgaria, 2000.
[28] A. Kucaba-Pietal, Application of boundary collocation method in fluid mechanics to stokes flow problems, Numer. Anal. Appl. Lecture Notes Comput. Sci. 2001 (1988) 498–505.
[29] J.A. Kolodziej, T. Strek, Analytical approximations of the shape factors for conductive heat flow in circular and regular polygonal cross-sections, Int. J. Heat Mass Transfer 44 (2001) 999–1012.
[30] M.S. Abou-Dina, Implementation of Trefftz method for the solution of some elliptic boundary value problems, Appl. Math. Comput. 127 (2002) 125–147.
[31] M.K. Moharana, P.K. Das, Heat conduction through heat exchanger tubes of noncircular cross-section, J. Heat Transfer 130 (2008). pp. 011301(1–8).
[32] M.K. Moharana, P.K. Das, Heat conduction through eccentric annuli: an appraisal of analytical, semi-analytical and approximate techniques, J. Heat Transfer 134 (2012). pp. 091301(1–9).
[33] S.J. Farlow, Partial Differential Equations for Scientists and Engineers, Dover publications Inc., Mineola, New York, 1993.
[34] M.U. Tyn, L. Debnath, Linear Partial Differential Equations for Scientists and Engineers, Birkhäuser, Boston, 2007.
[35] M.E. Steinke, S.G. Kandlikar, Single-phase liquid friction factors in microchannels, in: Proceedings of ICMM2005 Third International Conference on Microchannels and Minichannels, Toronto, Ontario, Canada, 2005.
[36] J. Happel, H. Brenner, Low Reynolds Number Hydrodynamics: With Special Applications to Particulate Media, Kluwer, Hague, Netherlands, 1983.
[37] F.M. White, Viscous Fluid Flow, Second ed., McGraw-Hill Inc., New York, USA, 1991.
[38] M. Spiga, G.L. Morini, A symmetric solution for velocity profile in laminar flow through rectangular ducts, Int. Comm. Heat Mass Transfer 21 (1994) 469–475.
[39] R. Begum, M. Zamir, Flow in tubes of non-circular cross-sections, in: M. Rahman (Ed.), Ocean Waves Mechanics, Computational Fluid Dynamics and Mathematical Modeling, Computational Mechanics Publications, Boston, 1990.
[40] P.K. Kundu, I.M. Cohen, Fluid mechanics, Third ed., Academic press, New Delhi, 2005.
[41] P.N. Shivakumar, Viscous flow in pipes whose cross-sections are doubly-connected regions, Appl. Sci. Res. 27 (1973) 355–365.
[42] W. Tiedt, Bereehnung des laminaren und turbulenten Reibungswiderstandes konzentrischer und exzentrisher Ringspalte. Part I. Chem.-Ztg., Chem. Appar., 90 (1966), pp. 813–821. (Part II. Chem.-Ztg., Chem. Appar. 91 (1997), pp. 17–25.)
[43] J.A. Kolodziej, R. Starosta, Self-adaptive Trefftz procedure for harmonic problems, Comp. Ass. Mech. Engrg. Sci. 4 (3–4) (1997) 491–500.